Journal of Applied Mathematics and Physics, 2025, 13(10), 3279-3292
https://www.scirp.org/journal/jamp
ISSN Online: 2327-4379
ISSN Print: 2327-4352

Diversity of Soliton Structures in (2 + 1)-Dimensional BKP Equation with Variable Coefficients

Keke Chen, Meiling Duan*

College of Mathematics and Statistics, Jishou University, Jishou, China
Email: *2570557275@qq.com

How to cite this paper: Chen, K.K. and Duan, M.L. (2025) Diversity of Soliton Structures in (2 + 1)-Dimensional BKP Equation with Variable Coefficients. *Journal of Applied Mathematics and Physics*, **13**, 3279-3292.
https://doi.org/10.4236/jamp.2025.1310188

Received: September 12, 2025
Accepted: October 25, 2025
Published: October 28, 2025

Abstract

The study derives the Hirota bilinear form for a variable-coefficient (2 + 1)-dimensional BKP equation and constructs *N*-soliton, *M*-lump, and mixed lump-soliton solutions. By testing four representative time-dependent coefficient sets, the authors visualise how $\alpha(t)$, $\beta(t)$ and $\delta(t)$ shape the spatial patterns of solitons and lumps. The work emphasises the richer structural diversity and evolution pathways that arise when coefficients vary with time.

Keywords

Variable Coefficients, Hirota's Bilinear Method, Soliton Structures, Interaction Behavior

1. Introduction

As one of the three major branches of nonlinear science, soliton theory has long been a focus of significant academic attention. Solitons, as special types of nonlinear localized waves, not only provide precise descriptions of wave phenomena in nature, but also demonstrate substantial application value across multiple disciplines, including fluid mechanics, theoretical physics, nonlinear optics, and ocean dynamics. Moreover, variable-coefficient nonlinear partial differential equations, owing to their enhanced capability to accurately characterize complex and dynamic nonlinear behaviors [1]-[6], endow this field of research with profound theoretical significance and promising application prospects. The (2 + 1)-dimensional B-type Kadomtsev-Petviashvili equation (BKP equation) is given as follows:

$$u_{yt} - u_{xxxy} - 3\left(u_x u_y\right)_x + \delta u_{xx} = 0. \tag{1}$$

Equation (1) represents a significant generalization of the KP equation, exhibiting richer mathematical structures and deeper physical implications. It finds broad applications across various nonlinear scientific fields, particularly in fluid dynamics, plasma physics, and nonlinear optics [7] [8]. Consequently, numerous researchers have employed diverse methodologies to conduct in-depth investigations into solution types of nonlinear differential equations. Substantial progress has been achieved in solving the BKP equation, successfully constructing a comprehensive system of analytical solutions, including soliton solutions, breather solutions, lump solutions, and various interaction solutions. These developments provide crucial theoretical tools for explaining nonlinear physical phenomena. For instance: Mao *et al.* [9] established the bilinear form of the (3 + 1)-dimensional BKP equation using binary Bell polynomials and constructed lump solutions with arbitrary self-similar parameters under the $z = x$ condition. Tang *et al.* [10] investigated the construction of exact solutions through Wronskian and Grammian techniques. Su *et al.* [11] obtained rational solutions, soliton solutions, and their interaction solutions for the generalized BKP equation based on Hirota's bilinear method. Na [12] derived analytical expressions for multi-soliton solutions by combining Bell polynomials with Bäcklund transformations. Hao *et al.* [13] systematically studied decomposed solutions and Lax pairs using a modified variable separation approach. Yang *et al.* [14] extended the bilinear operators and conducted in-depth analysis of the dynamical characteristics of lump solutions. Zhang *et al.* [15] developed n-th order rational solutions from N-soliton solutions via the long-wave limit method, and further investigated the collision dynamics of lump solutions in the (2 + 1)-dimensional BKP equation.

To investigate the diversity of soliton solutions and explore their spatial structures and dynamical properties, this study introduces variable coefficients into (1), yielding the following modified equation: In this paper, we consider the (2 + 1)-dimensional B-type Kadomtsev-Petviashvili equation as follows:

$$\alpha(t)u_{yt} - \beta(t)u_{xxxy} - 3\beta(t)\left(u_x u_y\right)_x + \delta(t)u_{xx} = 0, \tag{2}$$

The functions $\alpha(t), \beta(t)$ and $\delta(t)$ represent non-zero real differentiable functions of the temporal variable t. Current research on exact solutions and dynamical properties of constant-coefficient nonlinear partial differential equations has reached a relatively mature stage. However, the introduction of variable coefficients into nonlinear equations leads to significant variations in the forms of exact solutions. In particular, systematically obtaining exact solutions with specific patterns and characterizing their spatial structures using mathematical software such as Maple presents substantially increased complexity and difficulty. Consequently, studies on variable-coefficient nonlinear partial differential equations remain relatively scarce in the existing literature.

Against this background, this paper focuses on investigating the exact solutions of variable-coefficient nonlinear partial differential equations and the dynamical properties of their interaction solutions.

2. *N*-Solitons with Different Structures

This study employs the Hirota bilinear method to first derive the bilinear form of the (2 + 1)-dimensional BKP equation. We systematically investigate the characteristics and dynamical behaviors of *N*-soliton solutions for this equation under variable-coefficient conditions. In particular, by applying the long-wave limit technique combined with the parameter pairing complexification method, we successfully construct *M*th-order lump solutions from the *N*-soliton solutions. Following the framework established in reference [8] [16], we adopt the following form of parameter transformation:

$$u(x,y,t)=2(\ln f)_x \tag{3}$$

where $f=f(x,y,t)$ is a selected test function related to x, y and time variable t. Inserting (3) into (2)

$$P(D_x,D_y,D_t)f\cdot f=\left(\alpha(t)D_yD_t-\beta(t)D_x^3D_y+\delta(t)D_x^2\right)f\cdot f=0. \tag{4}$$

where D_x,D_y and D_t denote the bilinear differential operators. Based on the Hirota bilinear method, the form of the *N*-soliton is obtained.

$$f=f_N=\sum_{\varsigma=0,1}\exp\left(\sum_{s=1}^{N}\varsigma_s\Phi_s+\sum_{s<l}^{(N)}A_{sl}\varsigma_s\varsigma_l\right), \tag{5}$$

with

$$\begin{cases}\Phi_s=\omega_s\left(x+g_sy+h(t)\right)+\gamma_s,\\ h_s(t)=\int\dfrac{\beta(t)\omega_s^2g_s-\delta(t)}{\alpha(t)g_s}\mathrm{d}t,\\ e^{A_{sl}}=\dfrac{3\beta(t)g_sg_l(\omega_s-\omega_l)(\omega_sg_s-\omega_lg_l)+\delta(t)(g_s-g_l)^2}{3\beta(t)g_sg_l(\omega_s+\omega_l)(\omega_sg_s+\omega_lg_l)+\delta(t)(g_s-g_l)^2}.\end{cases} \tag{6}$$

where, ω_s,g_s are free parameters, where the $\sum_{\varsigma=0,1}$ represents summation over all possible combinations of $\varsigma_1=0,1,\varsigma_2=0,1,\cdots,\varsigma_N=0,1$, and the $\sum_{i<j}^{(N)}$ is over all possible combinations of the N elements with the specific condition $s<l$. By substituting (5) and (6) into (3), we obtain the *N*-soliton solutions of the equation. To investigate the influence of variable coefficients on the spatial evolution structure of the *N*-soliton solutions, we select several sets of variable coefficients and employ Maple software to visualize different types of *N*-soliton solutions in three-dimensional space.

Parameter (1): $\alpha(t)=2,\beta(t)=1,\delta(t)=3$,

Parameter (2): $\alpha(t)=\dfrac{1}{1+\sin(t)+\cos(t)},\beta(t)=1,\delta(t)=1$,

Parameter (3): $\alpha(t)=1,\beta(t)=t,\delta(t)=t$,

Parameter (4): $\alpha(t)=\dfrac{1}{t\cos(t)},\beta(t)=1,\delta(t)=1$.

By substituting the above parameters into (5) and (3), we obtain the *N*-soliton

solutions of the (2 + 1)-dimensional BKP equation. Selecting appropriate parameters allows us to plot the three-dimensional spatial structures of soliton solutions under different coefficients. Parameters a,b,c,d correspond to case Parameters (1), (2), (3), and (4). Through comparison of the soliton solution structures under these parameter sets, we can clearly observe that the variable-coefficient cases exhibit more complex spatial configurations. When $s=1$, the following parameters are selected to construct four distinct spatial configurations of the 1-soliton solution (see **Figure 1**). (a) $\omega_1=-\frac{1}{3}$, $g_1=\frac{3}{2}$; (b) $\omega_1=\frac{1}{3}$, $g_1=-1$; (c) $\omega_1=\frac{1}{4}$, $g_1=\frac{1}{2}$; (d) $\omega_1=-\frac{1}{8}$, $g_1=-1$.

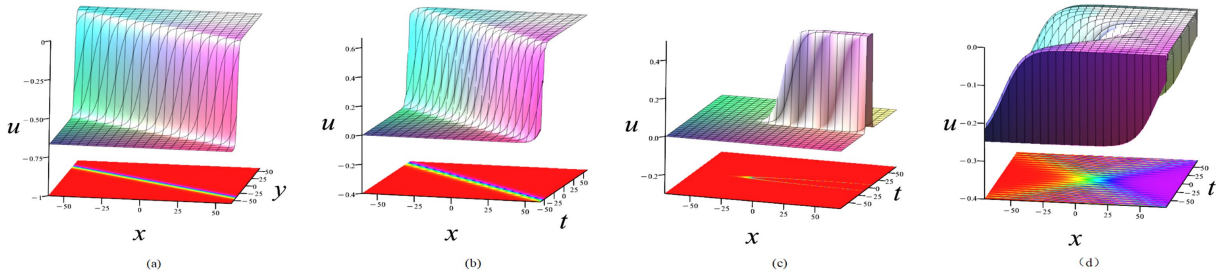

Figure 1. The three-dimensional profiles of the 1-soliton solution under four different coefficient conditions when $\gamma_1=0$. (a) $\alpha(t)=2$, $\beta(t)=1$, $\delta(t)=3$; (b) $\alpha(t)=\frac{1}{1+\sin(t)+\cos(t)}$, $\beta(t)=1$, $\delta(t)=1$; (c) $\alpha(t)=1$, $\beta(t)=t$, $\delta(t)=t$; (d) $\alpha(t)=\frac{1}{t\cos(t)}$, $\beta(t)=1$, $\delta(t)=1$.

When $s=2$, the following parameters are selected to construct four distinct spatial configurations of the 2-soliton solutions (see **Figure 2**). (a) $\omega_1=\frac{1}{5}$, $\omega_2=-\frac{1}{3}$, $g_1=-\frac{6}{5}$, $g_2=\frac{3}{2}$; (b) $\omega_1=-\frac{1}{2}$, $\omega_2=-\frac{3}{2}$, $g_1=1$, $g_2=1$; (c) $\omega_1=-\frac{1}{4}$, $\omega_2=-\frac{1}{8}$, $g_1=\frac{3}{2}$, $g_2=-\frac{2}{5}$; (d) $\omega_1=-\frac{1}{8}$, $\omega_2=\frac{3}{5}$, $g_1=-1$, $g_2=\frac{3}{2}$.

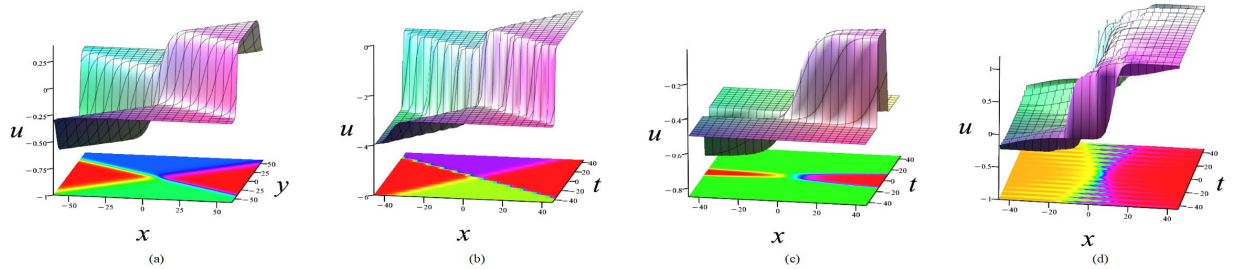

Figure 2. The three-dimensional profiles of the 2-soliton solutions under four different coefficient conditions when $\gamma_s=0(s=1,2)$. (a) $\alpha(t)=2$, $\beta(t)=1$, $\delta(t)=3$; (b) $\alpha(t)=\frac{1}{1+\sin(t)+\cos(t)}$, $\beta(t)=1$, $\delta(t)=1$; (c) $\alpha(t)=1$, $\beta(t)=t$, $\delta(t)=t$; (d) $\alpha(t)=\frac{1}{t\cos(t)}$, $\beta(t)=1$, $\delta(t)=1$.

When $s=3$, the following parameters are selected to construct four distinct spatial configurations of the 3-soliton solution (see Figure 3). (a) $\omega_1=\frac{1}{3}$, $\omega_2=\frac{1}{2}$, $\omega_3=-\frac{1}{3}$, $g_1=-\frac{2}{3}$, $g_2=\frac{5}{2}$, $g_3=\frac{1}{4}$; (b) $\omega_1=-\frac{1}{4}$, $\omega_2=-\frac{3}{2}$, $\omega_3=\frac{3}{4}$, $g_1=\frac{2}{3}$, $g_2=\frac{3}{5}$, $g_3=\frac{5}{4}$; (c) $\omega_1=-\frac{1}{4}$, $\omega_2=\frac{1}{4}$, $\omega_3=-\frac{1}{6}$, $g_1=\frac{5}{2}$, $g_2=\frac{1}{5}$, $g_3=-\frac{3}{2}$; (d) $\omega_1=-\frac{1}{4}$, $\omega_2=\frac{1}{2}$, $\omega_3=-\frac{1}{6}$, $g_1=\frac{5}{2}$, $g_2=\frac{3}{5}$, $g_3=-\frac{1}{2}$.

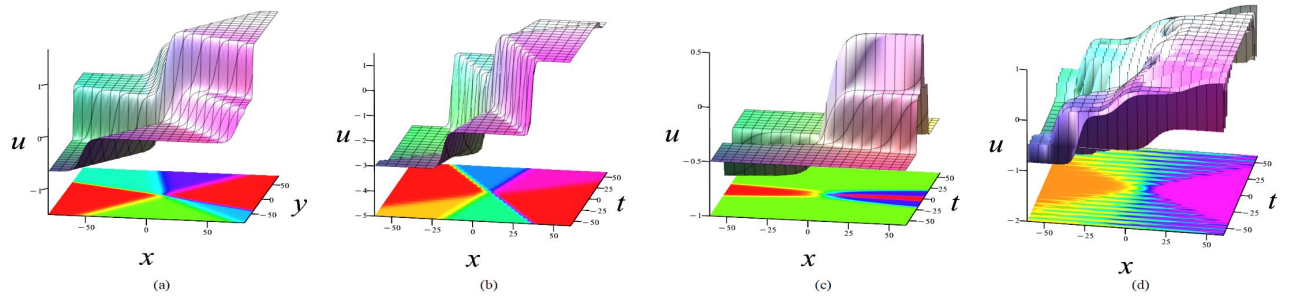

Figure 3. The three-dimensional profiles of the 3-soliton solutions under four different coefficient conditions when $\gamma_s=0\,(s=1,2,3)$. (a) $\alpha(t)=2$, $\beta(t)=1$, $\delta(t)=3$; (b) $\alpha(t)=\frac{1}{1+\sin(t)+\cos(t)}$, $\beta(t)=1$, $\delta(t)=1$; (c) $\alpha(t)=1$, $\beta(t)=t$, $\delta(t)=t$; (d) $\alpha(t)=\frac{1}{t\cos(t)}$, $\beta(t)=1$, $\delta(t)=1$.

3. Higer-Order Lump Solution

Based on the *N*-soliton solution, we first employ the long-wave limit method to derive the *N*-rational solution. Subsequently, by imposing pairwise complexification of parameters, we obtain the *M*-lump solutions for (2). To derive the *M*-lump solutions, we begin by setting: $\gamma_s=I\pi$, $\frac{\omega_s}{\omega_l}=O(1)$, $\omega_s\to 0$. Which yields the following *N*-rational solution form:

$$\begin{aligned}\tilde{F}_N=&\prod_{s=1}^{N}\theta_s+\frac{1}{2}\sum_{s,l}^{(N)}\Lambda_{sl}\prod_{i\neq s,l}^{N}\theta_i+\frac{1}{2!2^2}\sum_{s,l,k,q}^{(N)}\Lambda_{sj}\Lambda_{kq}\prod_{j\neq s,l,k,q}^{N}\theta_j+\cdots\\&+\frac{1}{M!2^M}\sum_{s,l,k,q,\cdots,m,n}^{(N)}\overbrace{\Lambda_{sl}\Lambda_{kq}\cdots\Lambda_{mn}}^{M}\prod_{r\neq s,t,k,q,\cdots,m,n}^{N}\theta_r+\cdots,\end{aligned}\tag{7}$$

with

$$\begin{cases}\theta_s=x+g_s y+\int\frac{-\delta(t)}{\alpha(t)g_s}\mathrm{d}t,\\ \Lambda_{sl}=-\frac{6\beta(t)g_s g_l(g_l+g_s)}{\delta(t)(g_l-g_s)^2}\end{cases}\tag{8}$$

where p_i are free parameters, and $\sum_{s,l,k,q,\cdots,m,n}^{(N)}$ denotes the summation over all possible combinations of s,l,k,q selected from $1,2,\cdots,2M$. By performing

pairwise complexification of parameters and selecting the following settings: $N=2M$, $g_s=c_s+d_s$, $g_{M+s}=g_s^*$, $(s=1,2,\cdots,M)$, we substitute these into (7) and (8). Finally, combining with the transformation (3), we obtain the M-lump solutions of the equation.

For the specific case of $N=2$:

$$\tilde{f}_2=\theta_1\cdot\theta_2+\Lambda_{12} \tag{9}$$

By substituting (9) back into (3), we obtain the 2-rational solutions of Equation (2). Subsequently, through parameter selection with $g_1=c_1+d_1$, $g_2=c_1-d_1$,we derive the 1-lump solution of Equation (2). By choosing appropriate parameters, we plot the spatial evolution diagrams of the first-order lump solution under different functional forms of $\alpha(t),\beta(t)$ and $\delta(t)$. With the parameter specification (1): When selecting parameters as $c_1=\frac{1}{2},d_1=-\frac{4}{5}$, we obtain three-dimensional spatial evolution plots at different time instances. Extensive research has been conducted by numerous scholars on lump solutions. As clearly demonstrated in **Figure 4**, for the constant-coefficient Parameter (1), the lump solution exhibits only translational motion in space over time while maintaining its structural integrity.

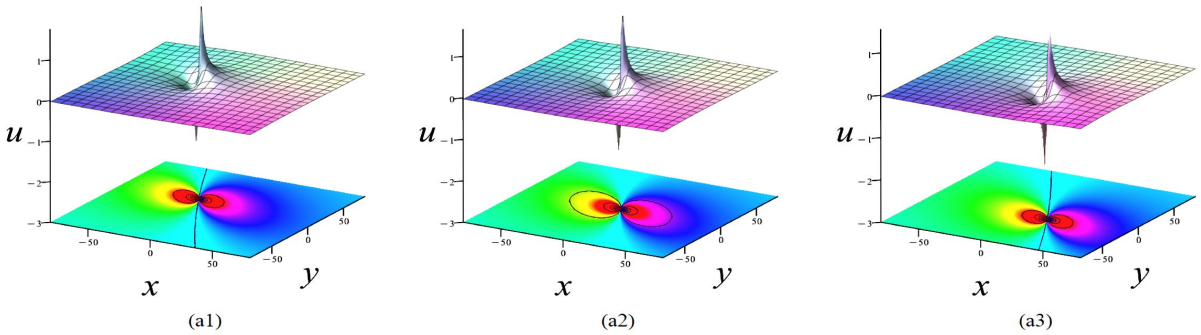

Figure 4. For the case where $\gamma_s=0,(s=1,2)$, figure panels (a1), (a2) and (a3) present the spatial evolution of the 1-lump solution under constant-coefficient conditions at three representative time instants: $t=-10$, $t=0$, and $t=10$, respectively. (a) $\alpha(t)=2$, $\beta(t)=1$, $\delta(t)=3$.

When selecting parameter set (b) $c_1=\frac{1}{9}$, $d_1=\frac{3}{4}$; (c) $c_1=\frac{1}{6}$, $d_1=-\frac{3}{5}$; (d) $c_1=\frac{1}{3}$, $d_1=2$, parameters b,c,d correspond to case Parameters (2), (3), and (4). We obtain three sets of spatial evolution diagrams for the variable-coefficient equation as it varies with y. For Parameter (2), the lump solution exhibits a single-peak-single-trough spatial structure similar to the constant-coefficient case. Along the y-direction, only spatial translation occurs while maintaining structural stability. With Parameter (3), both spatial configuration and position evolve significantly with y: the initial double-peak-double-trough pattern gradually transforms into a single-peak-single-trough structure before complete dissipation. This novel solution pattern under variable coefficients demonstrates distinct dynamic

behavior compared to conventional spatial evolutions. Notably, Parameter (4) yields more complex co-evolution of spatial configuration and position with y. Comparative analysis of these three cases reveals that parameter selection critically determines the solution's spatial characteristics, confirming the pronounced structural instability and morphological variability of lump solutions in variable-coefficient equations. See Figure 5.

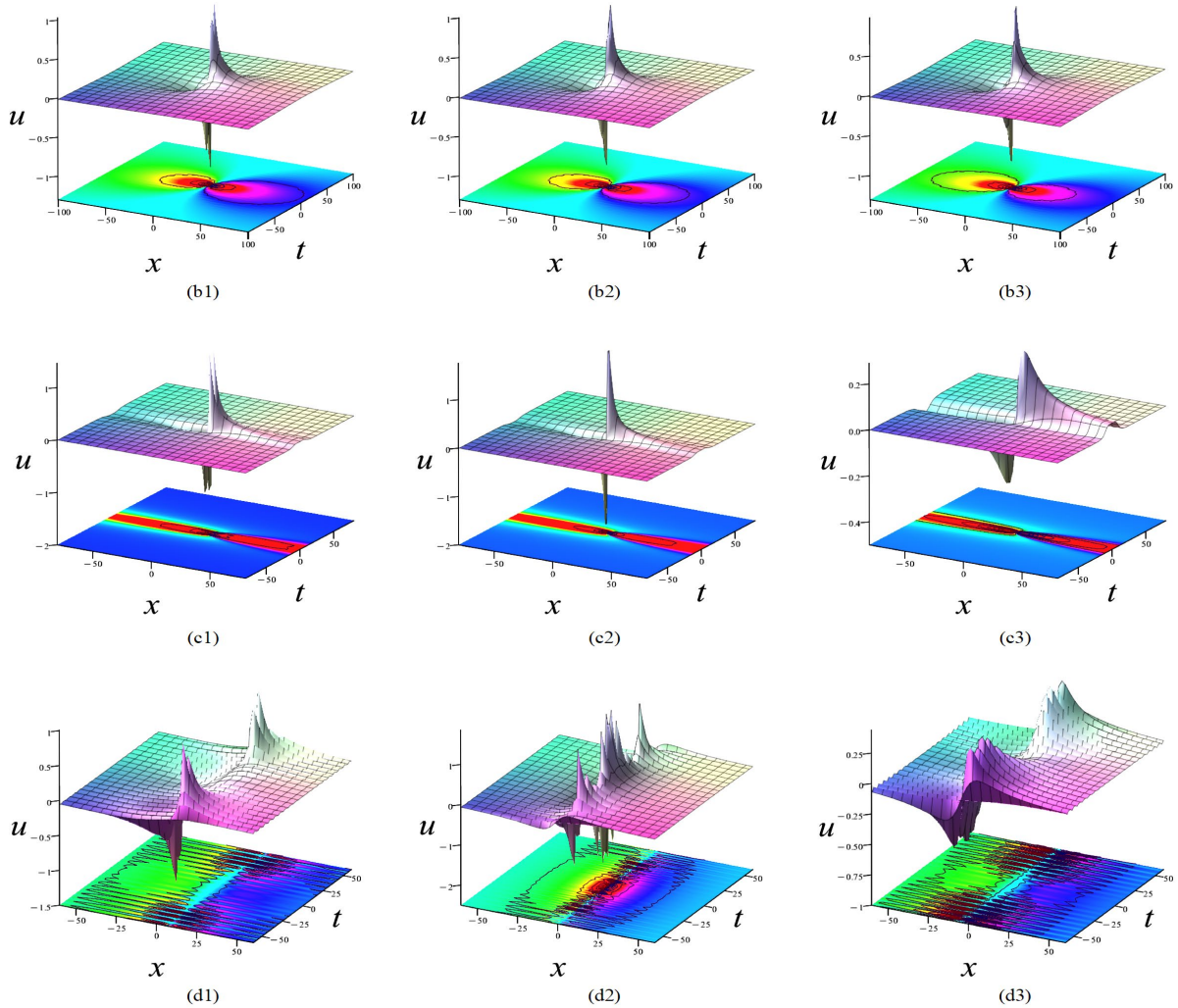

Figure 5. For the case where $\gamma_s = 0, (s = 1,2)$, figure panels ∂1, ∂2, ∂3 (∂ = b, c, d) present the spatial evolution of the 1-lump solution under variable-coefficient conditions at three representative time instants: $t = -10$, $t = 0$ and $t = 10$, respectively. (b) $\alpha(t) = \dfrac{1}{1+\sin(t)+\cos(t)}$, $\beta(t) = 1$, $\delta(t) = 1$; (c) $\alpha(t) = 1$, $\beta(t) = t$, $\delta(t) = t$; (d) $\alpha(t) = \dfrac{1}{t\cos(t)}$, $\beta(t) = 1$, $\delta(t) = 1$.

Similar to the derivation of the 1-lump solution, by setting $N = 4,6$ and substituting into (7), while taking the parameters as $g_{M+s} = g_s^*$, $g_s = c_s + d_s$, $(s = 1,2,\cdots,6)$, we obtain the 2- and 3-lump solutions of Equation (2). Here, we present the spatial structures of these solutions under both constant-coefficient

and various variable-coefficient conditions through appropriate parameter selections. When $N=4$, we illustrate the solutions by choosing suitable parameters: (a) $c_1=\frac{1}{2}$, $d_1=-\frac{8}{5}$, $d_1=-\frac{8}{5}$, $d_2=2$; (b) $c_1=-\frac{1}{6}$, $d_1=-\frac{3}{2}$, $c_2=-\frac{1}{2}$, $d_2=-2$; (c) $c_1=-\frac{2}{3}$, $d_1=-\frac{5}{3}$, $c_2=\frac{1}{4}$, $d_2=1$; (d) $c_1=-\frac{1}{7}$, $d_1=-\frac{3}{2}$, $c_2=-\frac{1}{3}$, $d_2=-\frac{4}{3}$, the various obtained 2-lump solutions are illustrated in Figure 6.

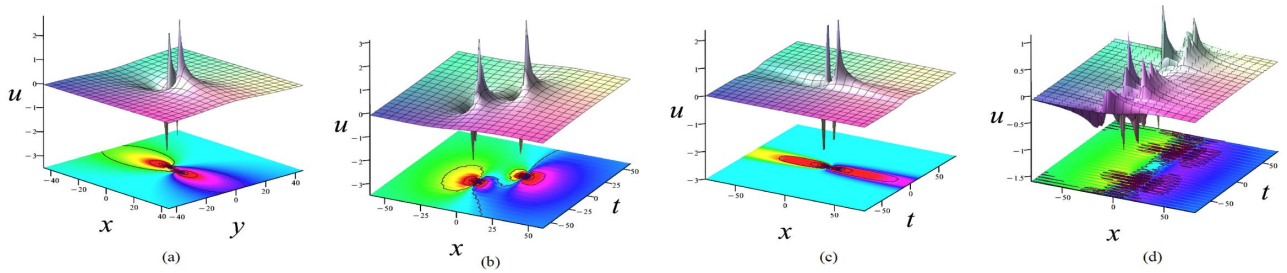

Figure 6. The spatial dynamics of 2-lump solutions are illustrated for four different parameter cases at $\gamma_s=0,(i=1,2,3,4)$. (a) $\alpha(t)=2$, $\beta(t)=1$, $\delta(t)=3$; (b) $\alpha(t)=\frac{1}{1+\sin(t)+\cos(t)}$, $\beta(t)=1$, $\delta(t)=1$; (c) $\alpha(t)=1$, $\beta(t)=t$, $\delta(t)=t$; (d) $\alpha(t)=\frac{1}{t\cos(t)}$, $\beta(t)=1$, $\delta(t)=1$.

When $N=6$,we illustrate the solutions by choosing suitable parameters: (a) $c_1=\frac{1}{4}$, $d_1=-\frac{1}{2}$, $c_2=-\frac{3}{5}$, $d_2=-2$, $c_3=-\frac{1}{4}$, $d_3=-\frac{5}{3}$; (b) $c_1=-\frac{1}{4}$, $d_1=-\frac{3}{2}$, $c_2=-\frac{3}{5}$, $d_2=-\frac{5}{3}$, $c_3=\frac{1}{6}$, $d_3=-\frac{3}{5}$; (c) $c_1=\frac{1}{2}$, $d_1=-\frac{2}{3}$, $c_2=\frac{3}{5}$, $d_2=-1$, $c_3=-\frac{2}{5}$, $d_3=-\frac{5}{4}$; (d) $c_1=-\frac{1}{7}$, $d_1=-\frac{3}{2}$, $c_2=-\frac{1}{3}$, $d_2=-\frac{4}{3}$, $c_3=\frac{1}{3}$, $d_3=-1$. The various obtained 3-lump solutions are illustrated in Figure 7.

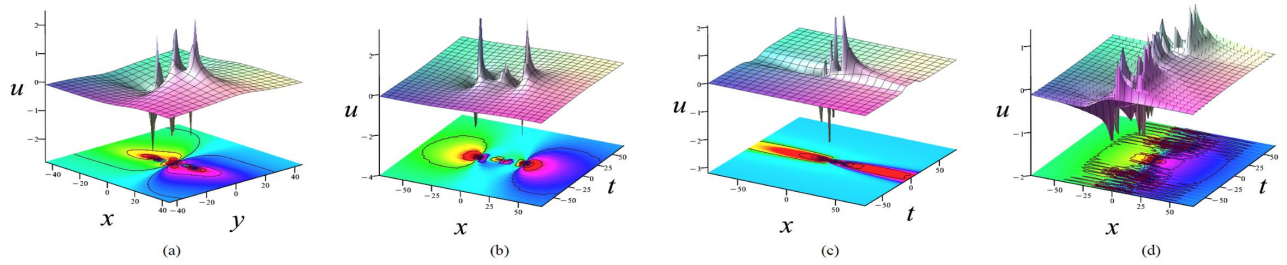

Figure 7. The spatial dynamics of 3-lump solutions are illustrated for four different parameter cases at $\gamma_i=0,(i=1,2,\cdots,6)$. (a) $\alpha(t)=2$, $\beta(t)=1$, $\delta(t)=3$; (b) $\alpha(t)=\frac{1}{1+\sin(t)+\cos(t)}$, $\beta(t)=1$, $\delta(t)=1$; (c) $\alpha(t)=1$, $\beta(t)=t$, $\delta(t)=t$; (d) $\alpha(t)=\frac{1}{t\cos(t)}$, $\beta(t)=1$, $\delta(t)=1$.

4. Interaction Solution

4.1. 1-Lump Solution with 1-Soliton Solution

To obtain the hybrid solution combining 1-lump and 1-soliton, we take $N=3$ and $\gamma_1=\gamma_2=I\pi$ in (5):

$$\begin{aligned} f_3 &= 1-e^{\Phi_1}-e^{\Phi_2}+e^{\Phi_1+\Phi_2+\Lambda_{12}} \\ &\quad +e^{\Phi_3}\left(1-e^{\Phi_1+\Lambda_{13}}-e^{\Phi_2+\Lambda_{23}}+e^{\Lambda_{12}+\Lambda_{12}+\Lambda_{12}+\Phi_1+\Phi_2}\right) \end{aligned} \tag{10}$$

where, Φ_i satisfies the parametric condition given in Equation (6). Then, by setting $\frac{\omega_1}{\omega_2}=0$ and taking the limits $\omega_1\to 0$, $\omega_2\to 0$ in (10), we obtain the following expression for $\dot{f}_3$:

$$\dot{f}_3=\theta_1\theta_2+\Lambda_{12}+e^{\Phi_3}\left(\theta_1\theta_2+\Lambda_{12}+\theta_1V_{23}+\theta_2V_{13}+V_{13}V_{23}\right) \tag{11}$$

with

$$\begin{cases} \theta_s = x+g_s y+\int\frac{-\delta(t)}{\alpha(t)g_s}\mathrm{d}t, \\ h_3(t)=\int\frac{\beta(t)\omega_3^2 g_s-\delta(t)}{\alpha(t)g_3}\mathrm{d}t, \\ \Lambda_{sl}=-\frac{6\beta(t)g_s g_l(g_l+g_s)}{\delta(t)(g_l-g_s)^2}, \\ V_{sl}=\frac{6\beta(t)\omega_l g_s g_l(g_l+g_s)}{3\beta(t)g_l^2 g_s\omega_l^2+\delta(t)g_l^2-2\delta(t)g_s g_l+\delta(t)p_s^2}, (s=1,2,l=3). \end{cases} \tag{12}$$

In (11) and (12), we select the parameters as $\omega_2=\omega_1^*=a_1+b_1$, $g_2=g_1^*=c_1+d_1$, and substitute them into the transformation (3) to obtain the hybrid 1-lump solution and 1-soliton solution of Equation (2). By choosing appropriate parameters, we present spatial profiles of the hybrid solutions for both constant and variable coefficients. The specific parameter values are given in **Figure 8**: (a) $c_1=-\frac{1}{3}$, $d_1=\frac{3}{4}$, $\omega_3=-\frac{1}{2}$, $g_3=-\frac{1}{3}$, $\gamma_3=0$.

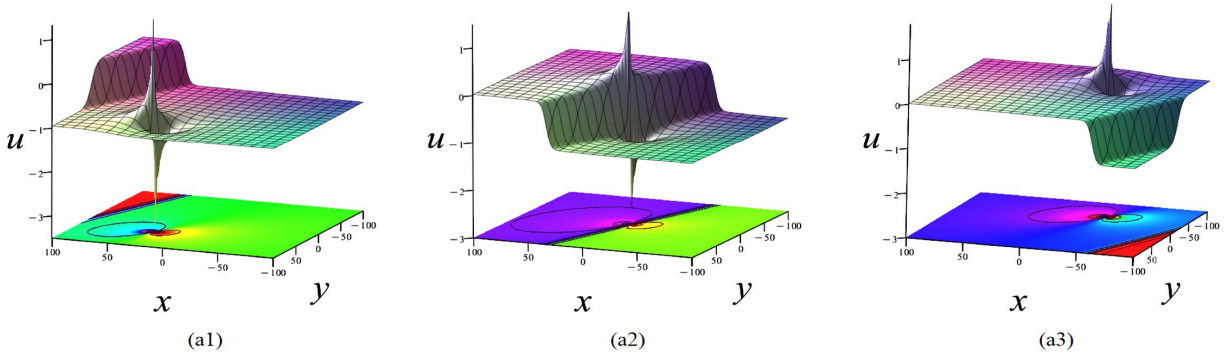

Figure 8. Three-dimensional evolution profiles of 1-lump and 1-soliton solutions with real coefficients at time instants. (a1) $t=-20$; (a2) $t=0$; (a3) $t=20$. (a) $\alpha(t)=2$, $\beta(t)=1$, $\delta(t)=3$.

When the parameter is taken as (b) $c_1=-\frac{1}{5}$, $d_1=\frac{2}{5}$, $\omega_3=-\frac{1}{2}$, $g_3=1$, $\gamma_3=0$; (c) $c_1=\frac{1}{5}$, $d_1=\frac{3}{5}$, $\omega_3=\frac{1}{2}$, $g_3=1$, $\gamma_3=0$; (d) $c_1=\frac{1}{2}$, $d_1=\frac{5}{2}$, $g_3=-\frac{1}{2}$, $g_3=1$, $\gamma_3=0$. The spatial evolution patterns of various hybrid 1-lump and 1-soliton solution are shown in Figure 9.

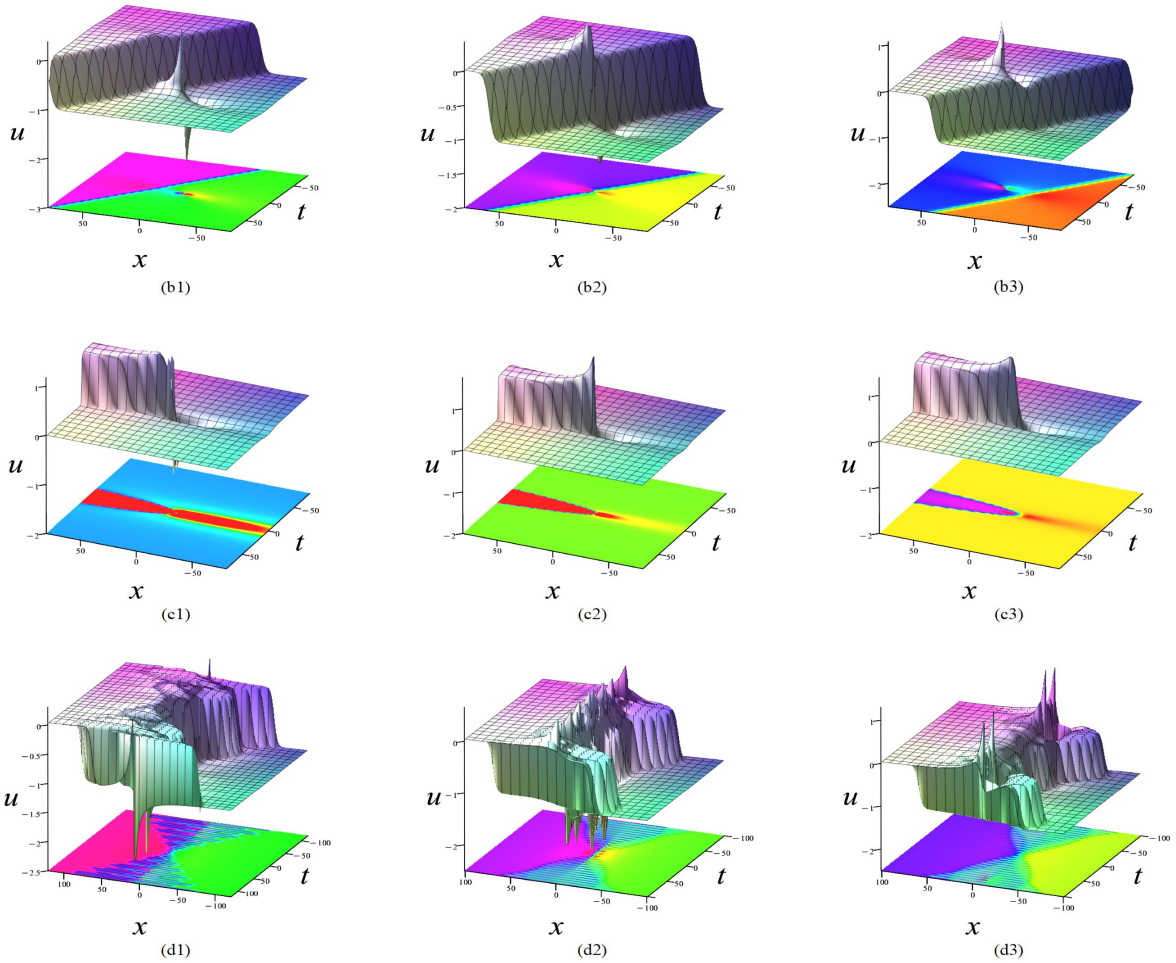

Figure 9. Three-dimensional profiles of 1-lump solution and 1-soliton solution under three variable-coefficient conditions. (b) $\alpha(t)=\frac{1}{1+\sin(t)+\cos(t)}$, $\beta(t)=1$, $\delta(t)=1$, $t=-20$, $t=0$, $t=20$; (c) $\alpha(t)=1$, $\beta(t)=t$, $\delta(t)=t$, $t=-10$, $t=0$, $t=10$; (d) $\alpha(t)=\frac{1}{t\cos(t)}$, $\beta(t)=1$, $\delta(t)=1$, $t=-10$, $t=0$, $t=10$.

4.2. 1-Lump Solution with 2-Soliton Solution

Following a similar methodology to the hybrid 1-lump and 1-soliton solution construction, we may derive the hybrid solution comprising 1-lump and 2-solitons. Based on Equation (5) with parameter selections $N=4$, $\gamma_1=I\pi$, $\gamma_2=I\pi$, then imposing the limits $\frac{\omega_1}{\omega_2}=0$, $\omega_1\to 0$, $\omega_2\to 0$ in (10), we obtain the following

expression for $\dot{f}_4$:

$$\begin{aligned}\dot{f}_4 &= \theta_1\theta_2 + \Lambda_{12} + e^{\Phi_3}\left(\theta_1\theta_2 + \Lambda_{12} + \theta_1 V_{23} + \theta_2 V_{13} + V_{13}V_{23}\right)\\ &+ e^{\Phi_4}\left(\theta_1\theta_2 + \Lambda_{12} + \theta_1 V_{24} + \theta_2 V_{14} + V_{14}V_{24}\right)\\ &+ e^{\Phi_3+\Phi_4+A_{12}}\left(\theta_1\theta_2 + \Lambda_{12} + \theta_1 V_{23} + \theta_2 V_{13} + V_{13}V_{23}\right)\end{aligned} \tag{13}$$

with

$$\begin{cases}\theta_s = x + g_s y + \int \dfrac{-\delta(t)}{\alpha(t) g_s}\mathrm{d}t,\\ h_3(t) = \int \dfrac{\beta(t)\omega_3^2 g_s - \delta(t)}{\alpha(t) g_3}\mathrm{d}t,\\ \Lambda_{sl} = -\dfrac{6\beta(t) g_s g_l (g_l + g_s)}{\delta(t)(g_l - g_s)^2},\\ V_{sl} = \dfrac{6\beta(t)\omega_l g_s g_l (g_l + g_s)}{3\beta(t) g_l^2 g_s \omega_l^2 + \delta(t) g_l^2 - 2\delta(t) g_s g_l + \delta(t) p_s^2}\\ e^{A_{34}} = \dfrac{3\beta(t) g_3 g_4 (\omega_3 - \omega_4)(\omega_3 g_3 - \omega_4 g_4) + \delta(t)(g_3 - g_4)^2}{3\beta(t) g_3 g_4 (\omega_3 + \omega_4)(\omega_3 g_3 + \omega_4 g_4) + \delta(t)(g_s - g_4)^2}, (s = 1,2, l = 3,4).\end{cases} \tag{14}$$

By selecting the parameters $\omega_{s+1} = \omega_1^* = a_s + b_s$, $g_{s+1} = g_s^* = c_s + d_s$, $(s = 1,2)$ and substituting them into transformation (3), we obtain the 1-lump and 2-soliton hybrid solution for Equation (2). Furthermore, by choosing appropriate parameter values, we present spatial profiles of the hybrid solutions under both constant-coefficient and variable-coefficient cases. The specific parameter selections are as follows: (a) $c_1 = \frac{1}{4}$, $d_1 = -\frac{1}{5}$, $p_3 = \frac{1}{5}$, $p_4 = -\frac{2}{3}$, $\omega_3 = \frac{2}{5}$, $\omega_4 = -\frac{1}{4}$, $\gamma_3 = 0$, $\gamma_4 = 0$. See Figure 10.

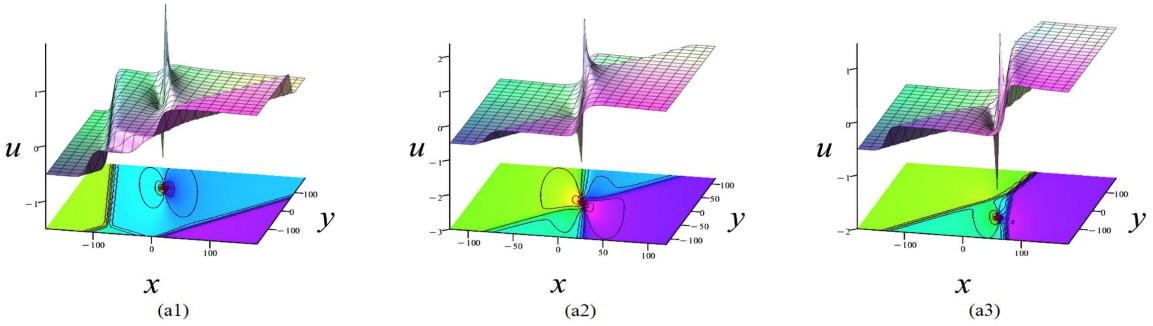

Figure 10. Three-dimensional evolution profiles of 1-lump solution and 2-soliton solutions with real coefficients at time instants. (a1) $t = -5$; (a2) $t = 0$; (a3) $t = 15$. (a): $\alpha(t) = 2$, $\beta(t) = 1$, $\delta(t) = 3$.

When the parameter is taken as (b) $c_1 = \frac{1}{2}$, $d_1 = \frac{5}{2}$, $g_3 = \frac{1}{2}$, $g_4 = -\frac{1}{4}$, $\omega_3 = \frac{1}{2}$, $\omega_4 = -\frac{1}{3}$, $\gamma_3 = 0$, $\gamma_4 = 0$; (c) $c_1 = \frac{1}{4}$, $d_1 = \frac{7}{2}$, $g_3 = \frac{1}{2}$, $g_4 = -\frac{1}{4}$, $\omega_3 = \frac{1}{2}$, $\omega_4 = -\frac{1}{3}$, $\gamma_3 = 0$, $\gamma_4 = 0$; (d) $c_1 = \frac{1}{2}$, $d_1 = \frac{5}{2}$, $g_3 = \frac{1}{2}$, $g_4 = -\frac{1}{4}$,

$\omega_3=\frac{1}{2}$, $\omega_4=-\frac{1}{3}$, $\gamma_3=0$, $\gamma_4=0$. The spatial evolution patterns of various hybrid 1-lump and 2-soliton solutions are shown in Figure 11.

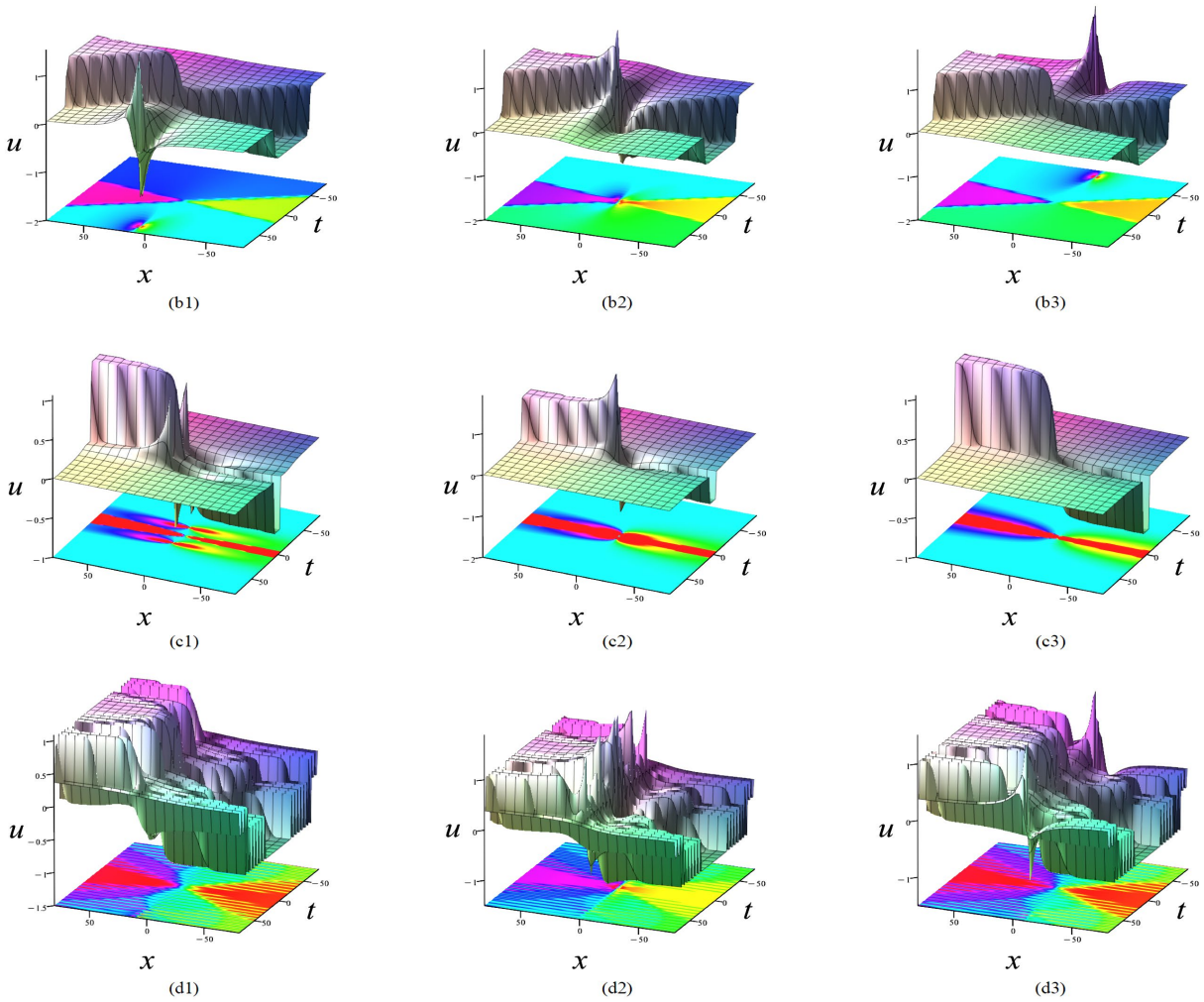

Figure 11. Three-dimensional profiles of 1-lump solution and 2-soliton solutions under three variable-coefficient conditions. (b) $\alpha(t)=\frac{1}{1+\sin(t)+\cos(t)}$, $\beta(t)=1$, $\delta(t)=1$, $t=-10$, $t=0$, $t=10$; (c) $\alpha(t)=1$, $\beta(t)=t$, $\delta(t)=t$, $t=-10$, $t=0$, $t=10$; (d) $\alpha(t)=\frac{1}{t\cos(t)}$, $\beta(t)=1$, $\delta(t)=1$, $t=-10$, $t=0$, $t=10$.

5. Conclusion

Employing Hirota's bilinear formalism, this study conducts a systematic investigation into the construction methodology of diverse exact solutions for the (2 + 1)-dimensional variable-coefficient BKP equation, where the *N*-soliton solutions are rigorously derived from the fundamental bilinear equation through direct computation, while the *M*-lump solutions and their nonlinear superposition with soliton solutions are successfully obtained by implementing the sophisticated long-wave limit technique combined with the complex conjugate parameter pairing strat-

egy, with all solution structures being meticulously visualized through three-dimensional spatial plots generated by Maple's symbolic computation platform under various configurations of time-dependent coefficient functions, and furthermore, by judiciously selecting appropriate parameter combinations, a comprehensive analysis is performed to elucidate the distinctive dynamical characteristics exhibited by these exact solutions under different physical scenarios.

Acknowledgements

This work has been supported by the National Natural Science Foundation of China (Grant No. 12461047), and the Scientific Research Project of the Hunan Education Department (Grant No. 24B0478).

Conflicts of Interest

The authors declare no conflicts of interest regarding the publication of this paper.

References

[1] Zhou, Y., Wang, M. and Wang, Y. (2003) Periodic Wave Solutions to a Coupled KdV Equations with Variable Coefficients. *Physics Letters A*, **308**, 31-36. https://doi.org/10.1016/s0375-9601(02)01775-9

[2] Hao, R., Li, L., Li, Z. and Zhou, G. (2004) Exact Multisoliton Solutions of the Higher-Order Nonlinear Schrödinger Equation with Variable Coefficients. *Physical Review E*, **70**, Article ID: 066603. https://doi.org/10.1103/physreve.70.066603

[3] Liu, W., Tian, B. and Zhang, H. (2008) Types of Solutions of the Variable-Coefficient Nonlinear Schrödinger Equation with Symbolic Computation. *Physical Review E*, **78**, Article ID: 066613. https://doi.org/10.1103/physreve.78.066613

[4] Demiray, H. (2009) Variable Coefficient Modified KdV Equation in Fluid-Filled Elastic Tubes with Stenosis: Solitary Waves. *Chaos, Solitons & Fractals*, **42**, 358-364. https://doi.org/10.1016/j.chaos.2008.12.014

[5] Chu, J., Liu, Y. and Chen, X. (2023) Integrability and Exact Solutions of the (2 + 1)-Dimensional Variable Coefficient Ito Equation. *Nonlinear Dynamics*, **112**, 1307-1325. https://doi.org/10.1007/s11071-023-09090-6

[6] Zhang, H., Zong, J., Tian, G. and Wei, G. (2024) Analysis of High-Order Bright-Dark Rogue Waves in (2 + 1)-D Variable-Coefficient Zakharov Equation via Self-Similar and Darboux Transformations. *Mathematics*, **12**, Article 1359. https://doi.org/10.3390/math12091359

[7] Zhao, Z. and Han, B. (2017) Lump Solutions of a (3 + 1)-Dimensional B-Type KP Equation and Its Dimensionally Reduced Equations. *Analysis and Mathematical Physics*, **9**, 119-130. https://doi.org/10.1007/s13324-017-0185-5

[8] Zhang, X., Wang, L., Chen, W., Yao, X., Wang, X. and Zhao, Y. (2022) Dynamics of Transformed Nonlinear Waves in the (3 + 1)-Dimensional B-Type Kadomtsev-Petviashvili Equation I: Transitions Mechanisms. *Communications in Nonlinear Science and Numerical Simulation*, **105**, Article ID: 106070. https://doi.org/10.1016/j.cnsns.2021.106070

[9] Mao, J., Tian, S., Zou, L., Zhang, T. and Yan, X. (2019) Bilinear Formalism, Lump Solution, Lumpoff and Instanton/Rogue Wave Solution of a (3 + 1)-Dimensional B-Type Kadomtsev-Petviashvili Equation. *Nonlinear Dynamics*, **95**, 3005-3017.

https://doi.org/10.1007/s11071-018-04736-2

[10] Tang, Y., Chen, Y. and Wang, L. (2014) Wronskian and Grammian Solutions for the (2 + 1)-Dimensional BKP Equation. *Theoretical and Applied Mechanics Letters*, **4**, Article ID: 013011. https://doi.org/10.1063/2.1401311

[11] Su, J. and Xu, G. (2016) New Exact Solutions for the (3 + 1)-Dimensional Generalized BKP Equation. *Discrete Dynamics in Nature and Society*, **2016**, Article ID: 5420156. https://doi.org/10.1155/2016/5420156

[12] Na, L. (2015) Bäcklund Transformation and Multi-Soliton Solutions for the (3 + 1)-Dimensional BKP Equation with Bell Polynomials and Symbolic Computation. *Nonlinear Dynamics*, **82**, 311-318. https://doi.org/10.1007/s11071-015-2159-1

[13] Hao, X. and Lou, S.Y. (2024) Decomposition Solutions and Bäcklund Transformations of the B-Type and C-Type Kadomtsev-Petviashvili Equations. *Communications in Theoretical Physics*, **76**, Article ID: 065004. https://doi.org/10.1088/1572-9494/ad3b8b

[14] Yang, X., Tang, L., Gu, X., Chen, W. and Tian, L. (2025) Lump and Interaction Solutions to a (3 + 1)-Dimensional BKP-Boussinesq-Like Equation. *Journal of Mathematical Analysis and Applications*, **543**, Article ID: 129030. https://doi.org/10.1016/j.jmaa.2024.129030

[15] Zhang, H., Geng, J. and Zhang, M. (2018) Rational Solutions and Bright-Dark Lump Solutions to the BKP Equation. *Modern Physics Letters B*, **32**, Article ID: 1850334. https://doi.org/10.1142/s0217984918503347

[16] Xu, Z., Chen, H. and Dai, Z. (2016) Kink Degeneracy and Rogue Potential Solution for the (3 + 1)-Dimensional B-Type Kadomtsev-Petviashvili Equation. *Pramana*, **87**, Article No. 31. https://doi.org/10.1007/s12043-016-1232-8